Acta Pharmaceutica Sinica B 2021;11(2):406–419

Chinese Pharmaceutical Association
Institute of Materia Medica, Chinese Academy of Medical Sciences

Acta Pharmaceutica Sinica B

www.elsevier.com/locate/apsb
www.sciencedirect.com

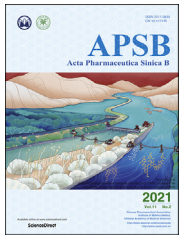

ORIGINAL ARTICLE

SUV39H1 deficiency suppresses clear cell renal cell carcinoma growth by inducing ferroptosis

Jianfeng Wang[a,†], **Xiaomao Yin**[a,†], **Wei He**[b,†], **Wei Xue**[a,*], **Jin Zhang**[a,*], **Yiran Huang**[a,*]

[a]*Department of Urology, Renji Hospital, School of Medicine, Shanghai Jiao Tong University, Shanghai 200127, China*
[b]*Department of Pathology, Renji Hospital, School of Medicine, Shanghai Jiao Tong University, Shanghai 200127, China*

Received 10 June 2020; received in revised form 20 August 2020; accepted 21 August 2020

KEY WORDS

Clear cell renal cell carcinoma;
SUV39H1;
Progression;
Prognostic model;
Ferroptosis;
DPP4;
Epigenetics;
Therapeutic target

Abstract Clear cell renal cell carcinoma (ccRCC) is a common kidney malignancy characterized by a poor prognosis. Suppressor of variegation 3–9 homolog 1 (*SUV39H1*), which encodes a histone H3 lysine 9 methyltransferase, has been reported to act as an oncogene in many cancers. However, it is unclear whether *SUV39H1* is involved in ccRCC. Here, we report that *SUV39H1* expression is frequently upregulated in ccRCC tumors and is significantly correlated with ccRCC progression. *SUV39H1* expression level is an independent risk factor for cancer prognosis, and integration with several known prognostic factors predicted ccRCC patient prognosis with improved accuracy than the conventional SSIGN (stage, size, grade and necrosis) prognostic model. Mechanistically, we discovered that siRNA knockdown or pharmacological inhibition of *SUV39H1* induced iron accumulation and lipid peroxidation, leading to ferroptosis that disrupted ccRCC cell growth *in vitro* and *in vivo*. We also show that *SUV39H1* deficiency modulated the H3K9me3 status of the *DPP4* (dipeptidyl-peptidase-4) gene promoter, resulting in upregulation of its expression that contributes to ferroptosis. Taken together, our findings provide the mechanistic insight into *SUV39H1*-dependent epigenetic control of ccRCC tumor growth and indicate that *SUV39H1* may serve as a potential therapeutic target for ccRCC treatment.

*Corresponding authors.
E-mail addresses: huangyiran@renji.com (Yiran Huang), med-zhangjin@vip.sina.com (Jin Zhang), uroxuewei@sjtu.edu.cn (Wei Xue).
†These authors made equal contributions to this work.
Peer review under responsibility of Chinese Pharmaceutical Association and Institute of Materia Medica, Chinese Academy of Medical Sciences.

https://doi.org/10.1016/j.apsb.2020.09.015

1. Introduction

Renal cell carcinoma (RCC) is the most common adult renal cancer originating from renal tubular epithelial cells[1]. Clear cell renal cell carcinoma (ccRCC) is the major histopathological RCC subtype, and accounts for approximately 75% of all RCC cases[2]. Localized ccRCC is generally cured by surgery, whereas patients with advanced ccRCC still face limited treatment options due to its intrinsic resistance to conventional chemotherapy or radiotherapy[3]. Recently, tremendous progress in our understanding of the underlying biology of this tumor type and the discovery of effective drugs have resulted in the development of several therapeutic methods, including immune-checkpoint inhibitors, vascular endothelial growth factor (VEGF) receptor tyrosine kinase inhibitors and mammalian target of rapamycin (mTOR) inhibitors, which have exhibited promising clinical results[4]. However, each of these management strategies has specific limitations, such as frequently occurring severe side effects and intrinsic or acquired drug resistance[5]. Clinicians therefore face a significant decision-making challenge when choosing the most appropriate therapeutic regimen for patients with advanced ccRCC. Thus, an individualized therapeutic regimen is desperately needed to provide hope for patients with advanced ccRCC.

Epigenetic alterations, such as histone modification, DNA methylation and the expression of non-coding RNAs, are closely involved in ccRCC initiation and progression, indicating that targeting the epigenome could be a promising approach to treating ccRCC[6,7]. Suppressor of variegation 3−9 homolog 1 (*SUV39H1*), a SET domain-containing histone methyltransferase (HMTase), is responsible for tri-methylation of histone 3 lysine 9 (H3K9me3), which is associated with heterochromatin formation and transcriptional repression of targeted genes[8]. *SUV39H1* is essential for mouse germ cell development and cell cycle regulation[9,10]. In addition, *SUV39H1* has been reported to participate in tumorigenesis in various types of cancer. *SUV39H1* is generally regarded as a tumor suppressor, due to its roles in suppressing genes required for proliferation and in promoting senescence[11]. However, increasing evidence indicates that *SUV39H1* may also serve as an oncogene in some human cancers. *SUV39H1* expression is upregulated in many cancers, including human colon carcinoma, bladder cancer and hepatocellular carcinoma, compared with nontumor tissues[12−14]. *SUV39H1* has been reported to function as an oncogene in melanoma *via* inhibiting the expression of retinoblastoma (RB)[15]. To date, the role of *SUV39H1* in ccRCC progression is still largely unknown.

Ferroptosis, an iron-dependent form of non-apoptotic regulated cell death, was originally identified in cancer cells with oncogenic *RAS* mutations[16]. Two central biochemical events, iron accumulation and lipid peroxidation, result in reactive oxygen species (ROS) production and subsequent cell death[17]. More importantly, ferroptosis has been implicated in the progression of neurodegenerative and neuropsychiatric diseases, ischemia−reperfusion injury and kidney degeneration[18]. Recent work has also indicated that dysfunction of ferroptosis is closely related to tumor progression. Inducing ferroptosis has emerged as an attractive strategy for managing various types of cancer[19]. Therefore, factors that regulate ferroptosis are potential therapeutic targets for cancer treatment. Dipeptidyl-peptidase-4 (DPP4, also known as CD26) is a glycoprotein mainly located at the plasma membrane that plays a critical role in regulating ferroptosis. In particular, DPP4 binds to NADPH oxidase 1 (NOX1) to form the DPP4−NOX1 complex, which facilitates intracellular lipid peroxidation and ultimately results in ferroptosis[20]. Of note, the expression levels of a variety of iron-related genes are significantly associated with ccRCC patient prognosis, suggesting that ferroptosis plays a vital role in ccRCC progression, and that targeting ferroptosis could be an effective option for ccRCC treatment[21].

In this study, we examined *SUV39H1* expression in ccRCC tumor tissues and analyzed its association with ccRCC progression and prognosis. Further, *SUV39H1* expression and *SUV39H1* activity were inhibited by genetic knockdown and pharmacological inhibition, respectively, to determine the functional role of *SUV39H1* in ccRCC cell growth both *in vitro* and *in vivo*. Finally, we investigated the exact mechanism underlying the effects of *SUV39H1* on ccRCC tumor growth. Our study provides proof-of-concept that targeting an epigenetic factor could be a promising strategy for ccRCC treatment.

2. Materials and methods

2.1. Patients and tissue samples

Two ccRCC patient cohorts for which clinical information was available were used for the analysis. For the first cohort, ClinicalMatrix and RNA sequencing data (HiSeqV2) for 534 ccRCC patients were obtained from the Cancer Genome Atlas (TCGA, https://cancergenome.nih.gov/) data portal. Patients for whom clinical information was missing were excluded when analyzing the relationship between *SUV39H1* expression level and clinical characteristics. The median mRNA expression value was considered as the cutoff value for low/high expression of *SUV39H1* or *DPP4* in ccRCC samples. For the second cohort, *SUV39H1* expression in ccRCC tumor and normal tissue samples from 358 patients (for whom follow-up data was available) was analyzed by immunohistochemistry (IHC). Overall survival (OS) was calculated from the time of surgery to the latest follow-up or death for any reason, while recurrence-free survival (RFS) was calculated from the date of nephrectomy to the date of recurrence. Tissues samples collected from ccRCC patients who had undergone nephrectomy were used for mRNA or protein extraction and IHC staining. Written consent was obtained from all the patients for sample collection. This study was approved by the Ethics and Research Committees of Renji Hospital, Shanghai Jiao Tong University School of Medicine, Shanghai, China.

2.2. RNA isolation and RT-qPCR

Total RNA was isolated using Trizol and reverse transcribed into cDNA following the manufacturer's instructions. Gene expression levels were measured by reverse transcription quantitative polymerase chain reaction (RT-qPCR) using ChamQ Universal SYBR qPCR Master Mix (Vazyme, Nanjing, China) and an ABI ViiA™ 7 System (Thermo Fisher, Waltham, MA, USA). Primers used in our study are listed in Supporting Information Table S1.

2.3. Western blot

Western blot analysis was performed as previously described[22]. Briefly, after collecting protein lysates in 2% SDS, we measured the protein concentration of each sample and separated the

samples on a 7.5%−12.5% SDS-PAGE gel (Bio-Rad Laboratories Inc., Hercules, CA, USA). Next, the proteins were transferred to a membrane, the membrane was blocked and then treated with various antibodies (with washing between steps), and target protein bands were detected by an enhanced chemiluminescence system (GE Healthcare Life Sciences, Chalfont, UK). All antibodies used in this study are listed in Supporting Information Table S2.

2.4. Immunohistochemistry

Tissue microarrays (TMAs) were constructed and stained as previously described[23]. A primary anti-SUV39H1 antibody was used for IHC staining. Tissue staining intensity and percentage were scored, and a comprehensive score (staining percentage × intensity) was used to evaluate the expression level of SUV39H1. A comprehensive score of 6 was set as the cutoff value to define low/high SUV39H1 expression in ccRCC tissues[24].

2.5. Cell culture and chemical reagents

RCC cell lines 786-O, Caki-1, A498, 769-P and ACHN and the normal cell line HK-2 were obtained from the American Type Culture Collection (Manassas, VA, USA). All cell lines were cultured in the recommended medium supplemented with 10% heat-inactivated fetal bovine serum (FBS, Gibco, Australia) at 37 °C with 5% CO_2. Chemical reagents, including ferrostatin-1 (CSN12654), z-VAD-FMK (CSN19230), necrostatin 1 (CSN11637), bafilomycin A1 (CSN10374), VX-765 (CSN15837), UNC0638 (CSN16350) and chaetocin (CSN19229) were provided by CSNpharm (Chicago, IL, USA).

2.6. Small interfering RNA (siRNA) transfection

Cells were seeded into plates at an appropriate density. After 12 h, small interfering RNAs (siRNAs, 50−100 nmol/L) and lipofectamine RNAiMAX transfection reagent (Invitrogen, Carlsbad, CA, USA) were added, according to the manufacturer's instructions. Western blotting was performed to detect the efficiency of gene knockdown. The sequence-specific siRNAs used to knock down *SUV39H1* and *DPP4* expression are listed in Supporting Information Table S3.

2.7. Cell proliferation assay

The effects of siRNA transfection and treatment with various compounds on cellular proliferation were determined by SulforhodamineB (SRB) assay according to the manufacturer's instructions. In brief, ccRCC cells were seeded into 96-well plates (1×10^3 cells/well) and incubated overnight at 37 °C. After treatment, cells were fixed, stained, and Soft Max pro plate reader was used to assess the cell viability at 560 nm.

2.8. Colony growth assay

Cells were seeded in 6- or 12- or 24-well plates at an appropriate density and incubated overnight at 37 °C. After managements, colony cell growth was measured at Day 3 or 7, and the colonies were fixed, stained, photographed and counted.

2.9. Cell cycle assay

Cell cycle analysis after siRNAs and drug treatments were performed by flow cytometry (Becton−Dickinson, Franklin Lakes, NJ, USA) as previous reported[22]. Briefly, cells were collected, fixed, stained with propidium iodide (PI) and analyzed by flow cytometry. The results were analyzed using ModFit software.

2.10. Lentiviral vector construction and transfection

Lentiviral particles were constructed as described[25]. In brief, a short hairpin RNA (shRNA) homologous to *SUV39H1* or a control shRNA was integrated into the pGMLV-SC5 backbone. The shRNA sequences are listed in Supporting Information Table S4. Cells were infected and subjected to puromycin selection before the experiments were performed.

2.11. Animal xenograft models and treatment

Female SCID mice (4−6 weeks old) were purchased and used for the xenograft models. Approximately 5×10^6 ccRCC cells were injected subcutaneously into the flank, or patient-derived tumor xenograft (PDX) was established using human ccRCC tissue (PDX#1002523691) from patients from Renji Hospital, with written patient consent. Tumor volume was estimated as Eq. (1):

$$\text{Tumor volume} = \text{Length} \times \text{Width}^2/2 \quad (1)$$

The mice were treated with vehicle (control) or chaetocin (0.5 mg/kg/day) by daily intraperitoneal injection. Mice body weights and tumor volumes were measured twice a week. After treatment, the tumors were harvested, weighed, photographed and fixed with 4% formaldehyde. Animal studies were performed in accordance with the guidelines of the Experimental Animal Ethics Committee of Shanghai Jiao Tong University (Shanghai, China).

2.12. Lipid ROS assay

Lipid ROS in cells was detected with C11-BODIPY (Cat. #D3861, Thermo Fisher) following the manufacturer's protocols. Briefly, after 2 days of treatment, cells were incubated with 10 μmol/L of C11-BODIPY and incubated in the dark at 37 °C, 5% CO_2 for 30 min. After washing three times with PBS, the C11-BODIPY green fluorescence (484 nm/510 nm) was measured with a flow cytometer.

2.13. Mitochondrial superoxide measurement

Mitochondrial superoxide production in ccRCC cells was detected using MitoSOX™ Red Mitochondrial Superoxide Indicator for live-cell imaging (Invitrogen) according to the manufacturer's protocols. After 2 days of treatment, the cells were stained with 5 μmol/L MitoSOX reagent in PBS for 10 min at 37 °C, 5% CO_2 in the dark, and then washed three times to remove excess MitoSOX. Cellular fluorescence was examined at an excitation/emission value of 510 nm/580 nm.

2.14. Iron assay

An Iron Assay Kit (Sigma−Aldrich, St. Louis, MO, USA) was used to measure the Fe^{2+} and total iron content of cells, according to the manufacturer's protocols. After 2 days of treatment, cells (5×10^6) were homogenized in 300 μL of iron assay buffer and

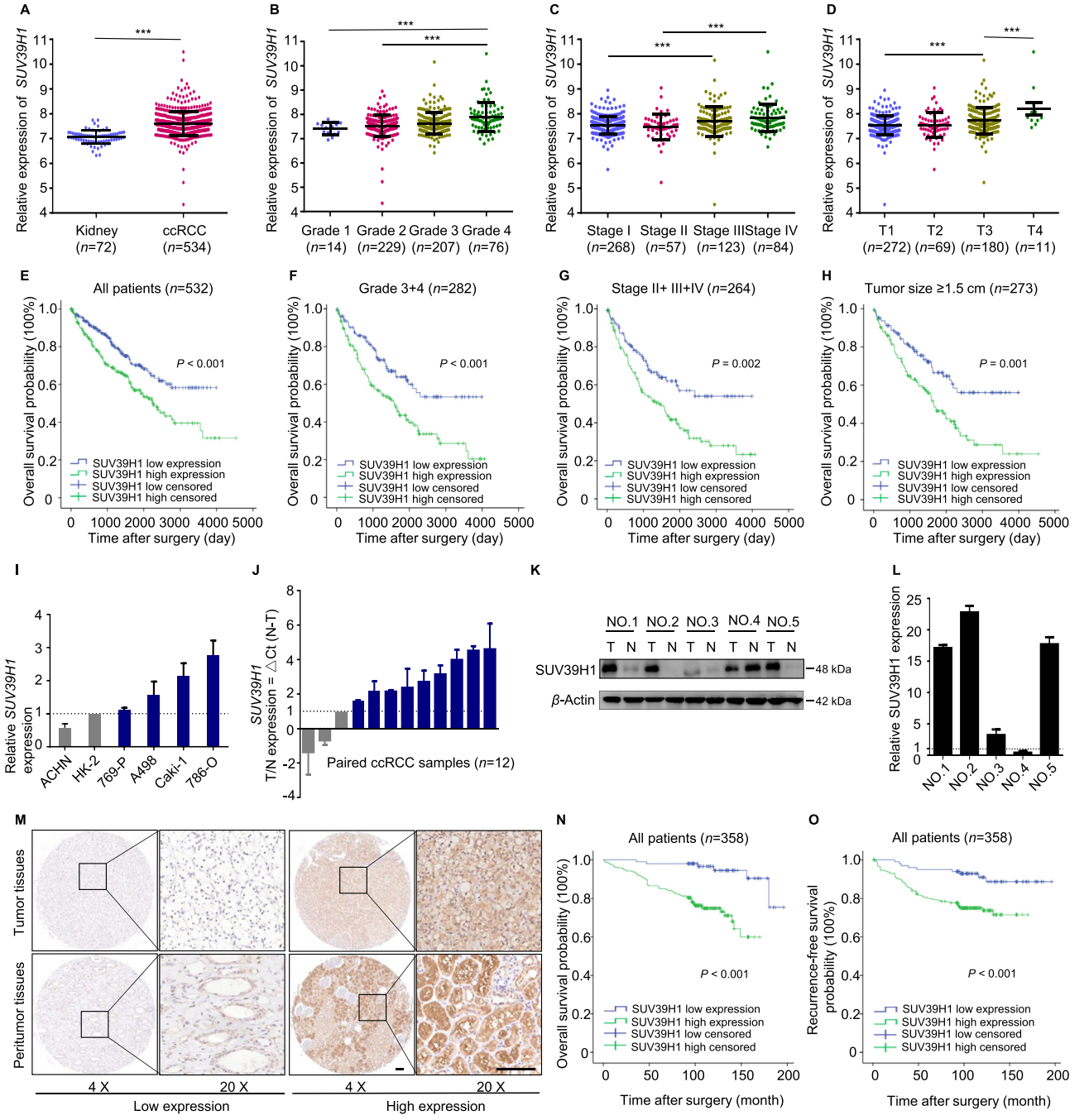

Figure 1 *SUV39H1* expression is upregulated in tumors and correlates with the progression and prognosis of ccRCC patients. (A) The mRNA levels of *SUV39H1* were analyzed in the ccRCC tissues in TCGA dataset compared to the normal controls. (B)−(D) The mRNA levels of *SUV39H1* in different histological grades, clinical TNM stages and T stages of ccRCC tissues. Patients with clinical information missing were excluded. (E) Kaplan−Meier analysis of OS for all ccRCC patients with low or high *SUV39H1* expression level in TCGA dataset. (F) Kaplan−Meier analysis of OS for patients with high histological grade (Grades 3+4). (G) Kaplan−Meier analysis of OS for patients with intermediate and advanced tumor stage (Stages II+III+IV). (H) Kaplan−Meier analysis of OS for patients with large tumor size (tumor size $\geq$ 1.5 cm). (I) RT-qPCR experiment was performed to analyze the *SUV39H1* mRNA level in ccRCC cell lines (786-O, Caki-1, A498, 769-P, and ACHN) and the normal kidney cell line HK-2. The expression level of β-actin was used as the normalized control. The experiment was repeated three times and data was presented as mean ± SD. (J) The mRNA level of *SUV39H1* was detected in 12 pairs of human ccRCC tumor tissues and adjacent normal tissues. The expression level of β-actin was used as normalized control. The experiment was repeated three times and data was presented as mean ± SD. (K) and (L) Western blot experiment was performed to evaluate the protein level of SUV39H1 in 5 paired ccRCC tissue samples, and β-Actin was used as control. The statistical analysis comes from technical replicates and the experiment was repeated three times. ("T" means tumor tissue and "N" means paired normal tissue). Data was presented as mean ± SD. (M) Representative images of SUV39H1 staining with high or low expression level in ccRCC tumor tissues and peritumor tissues. $n_{\text{Tumor tissues}} = 358$, $n_{\text{Peritumor tissues}} = 233$. Scale bar: 100 μm. (N) Kaplan−Meier analysis of ccRCC OS based on SUV39H1 expression level in ccRCC TMAs. $n = 358$. (O) Kaplan−Meier analysis of ccRCC RFS based on SUV39H1 expression level in ccRCC TMAs. $n = 358$. ***$P < 0.001$.

centrifuged at 16,000×*g* for 10 min at 4 °C. Next, 50 μL of the samples were transferred to a 96-well plate, and the volume was brought to 100 μL per well with assay buffer. To measure Fe^{2+}, 5 μL of iron assay buffer was added to each sample. To measure total iron, 5 μL of iron reducer was added to samples. Then, the 96-well plate was incubated for 30 min at room temperature. Next, 100 μL of iron probe was added to each sample, and the samples were then incubated in the dark for 60 min at room temperature. Finally, the absorbance was measured at 593 nm (A_{593}).

2.15. *RNA-sequencing analysis*

RNA-sequencing (RNA-seq) analysis was performed as described previously[26]. Briefly, cells were collected, and total RNA was isolated. RNA-seq was performed on the Illumina HiSeq2000, the data were aligned to the UCSC human hg19 genome using STAR 2.5, and hits were quantified using feature count software. The R package tools "DESeq2" and "ClusterProfiler" were used to analyze the RNA-seq data, using a fold change of 2 and an adjusted *P* value of 0.01 as the cut-off values, respectively.

2.16. *Chromatin immunoprecipitation analysis (ChIP)*

ChIP analysis was performed using a ChIP Kit from Cell Signal Technology (Cat. No. #9005, Danvers, MA, USA) according to the manufacturer's instructions. The percentage of *DPP4* gene promoter copies bound to H3K9me3 was quantified by qPCR using *DPP4* promoter-specific primers (Supporting Information Table S5).

2.17. *Statistical analysis*

Statistical analysis was performed using SPSS 22 software, R software or Graphpad Prism 6.0 (La Jolla, CA, USA). The chi-square function of SPSS 22 was used to investigate the correlations between SUV39H1 expression and clinical features, and the Kaplan−Meier method and log-rank test were used to analyze survival curves. The "rms" tool of R was used to analyze the nomograms, calibration plots, Harrell concordance index (C-index) and Akaike information criteria (AIC). Data was presented as mean ± standard deviation (SD), and a student's *t*-test was performed to calculate the statistical significance of differences between groups using GraphPad Prism. $^{*}P < 0.05$, $^{**}P < 0.01$ and $^{***}P < 0.001$ were considered significantly different.

3. Results

3.1. *SUV39H1 expression is upregulated in ccRCC tumors and correlates with the progression and prognosis*

Studies have indicated that *SUV39H1* plays a vital role in the progression of multiple cancers[12,14]. To assess the clinical role of *SUV39H1* in ccRCC progression, we first investigated the expression pattern of *SUV39H1* in ccRCC by analyzing publicly available data from TCGA. As shown in Fig. 1A, *SUV39H1* expression was significantly higher in ccRCC tumor tissues than that in normal tissues. *SUV39H1* expression was also correlated with various features of tumor progression, including histological grade, clinical TNM stage, invasion depth (T stage) and tumor size (Fig. 1B−D, Supporting Information Fig. S1A−S1C and Table S6).

A survival analysis was performed to investigate the prognostic value of *SUV39H1* expression level in ccRCC, and the results show that patients exhibiting high *SUV39H1* expression had significantly shorter OS than those with low *SUV39H1* expression (Fig. 1E). Moreover, *SUV39H1* expression level had significant prognostic value for ccRCC with a high histological grade (Grades 3+4), intermediate and advanced tumor stages (Stages II+III+IV), large tumors (tumor size ≥ 1.5 cm), deep invasion (T2+T3+T4), and negative for lymph node metastasis (N0 stage), while there was no significant prognostic value for patients with distant metastasis (Fig. 1F−H and Fig. S1D−S1L).

To further investigate *SUV39H1* expression in ccRCC, RT-qPCR and Western blot experiments were performed with ccRCC cell lines and paired normal and ccRCC tissue samples from patients. The results show that most ccRCC cell lines (786-O, Caki-1, A498, and 769-P) have a higher *SUV39H1* expression levels than the normal kidney cell line HK-2 (Fig. 1I). Consistent with this, ccRCC tumor tissues exhibited increased levels of *SUV39H1* mRNA and protein compared with normal tissues (Fig. 1J−L).

Next, we evaluated the SUV39H1 expression in ccRCC by performing an IHC staining analysis of a TMA consisting of 358 ccRCC tissue samples. As shown in Fig. 1M, variable SUV39H1 staining intensity was detected both in tumor tissues and paired peritumor tissues. Upregulated SUV39H1 expression was also observed in ccRCC tissues compared with peritumor tissues (Fig. S1M and S1N). The association between patients' clinicopathological features and SUV39H1 levels are summarized in Table 1. Of note, SUV39H1 expression was positively associated with clinical stage ($P = 0.020$), invasion depth (T stage, $P = 0.040$) and Fuhrman grade ($P = 0.002$). Furthermore, survival analysis indicated that a high level of SUV39H1 expression was significantly correlated with shorter OS and RFS in ccRCC patients (Fig. 1N and O). Taken together, these findings suggest that SUV39H1 expression is increased in ccRCC tumors and correlates with the progression and prognosis.

3.2. *Construction of nomogram models for predicting ccRCC patient prognosis*

We next investigated whether SUV39H1 expression level is an independent prognostic factor for ccRCC patient outcomes. Significant prognostic factors ($P < 0.05$) identified by univariate analysis were further assessed by multivariate analysis. The results indicate that SUV39H1 expression level, as well as TNM stage, Fuhrman grade and tumor size, was an independent prognostic predictor for OS and RFS of ccRCC patients (Table 2).

To evaluate the predictive value of SUV39H1 expression levels, C-index and AIC analyses were performed[27]. As shown in Table 3, the C-index values were increased and the AIC values were decreased for OS or RFS when SUV39H1 expression level was considered together with conventional prognostic factors, suggesting the SUV39H1 expression level has good predictive ability for ccRCC prognosis. Moreover, compared with the SSIGN outcome algorithm, the nomogram model integrating all factors (SUV39H1 expression, TNM stage, Fuhrman grade and tumor size) has a higher C-index and a lower AIC, which means that the nomogram model performed better than the conventional SSIGN outcome algorithm in predicting ccRCC prognosis.

To further assess the utility of SUV39H1 expression as a prognostic factor, we constructed two nomogram models to predict ccRCC patient prognosis by integrating all of the independent

Table 1 Association of SUV39H1 expression with clinicopathological characteristics of 358 ccRCC patients in TMAs.

Characteristic		Patient		SUV39H1 expression		*P*
		n	%	Low	High	
All patients		358	100	99	259	
Gender						0.950
	Male	254	70.9	70	184	
	Female	104	29.1	29	75	
Age (years)						0.259
	≤55	178	49.7	54	124	
	>55	180	50.3	45	135	
Stage						0.020*
	I+II	341	95.3	99	242	
	III+IV	17	4.7	0	17	
T stage						0.040*
	T1+T2	344	96.1	99	245	
	T3+T4	14	3.9	0	14	
N stage						0.133
	N0	349	97.5	99	250	
	N1	9	2.5	0	9	
M stage						0.286
	M0	352	98.3	99	253	
	M1	6	1.7	0	6	
Fuhrman grade						0.002*
	G1+G2	297	83.0	92	205	
	G3+G4	61	17.0	7	54	
Tumor size (cm)						0.280
	≤4	186	52.0	56	130	
	>4	172	48.0	43	129	

*$P < 0.05$ indicates a significant association among the variables.

prognostic predictors identified by the multivariate analysis[28]. Patients' OS or RFS probabilities could be predicted from the total score, which was calculated by adding up the points for each parameter (Supporting Information Fig. S2A and S2B). The calibration plots for the probability of OS or RFS at 3, 5, 7 and 10 years after surgery show good consistency between observed survival and that predicted by the nomogram models (Fig. S2C−S2J). Moreover, analysis of ccRCC data from TCGA largely supported our findings (Supporting Information Tables S7 and S8, and Fig. S2K−S2O). Our results suggest that these two nomogram models may be used to reliably predict the probable prognosis of ccRCC patients.

3.3. SUV39H1 knockdown inhibits ccRCC tumor growth and induces ferroptosis

Based on our finding that *SUV39H1* expression is correlated with ccRCC prognosis, we next investigated the functional role of *SUV39H1* in ccRCC cells. We initially evaluated the correlation between *SUV39H1* expression level and expression of *KI67*, a marker that is closely associated with tumor malignancy. As expected, *SUV39H1* expression was significantly correlated with *KI67* expression ($R = 0.4099$, $P < 0.001$) in ccRCC tumors from TCGA (Supporting Information Fig. S3A). To further investigate the effect of *SUV39H1* on ccRCC growth, *SUV39H1* was depleted by siRNAs in ccRCC cells, and the knockdown efficiency was assessed by Western blot (Fig. 2A). Compared with the negative control, cells in which *SUV39H1* expression was knocked down showed reduced growth and colony formation (Fig. 2B−E) and the cells were arrested in G2/M phase (Fig. 2F and G and Fig. S3B−S3C). We also employed a ccRCC cell-derived xenograft mouse model to investigate whether *SUV39H1* expression is essential for tumor growth *in vivo*. Caki-1 cells with stable depletion of *SUV39H1* significantly impaired tumor growth, as indicated by tumor volume, weight and size (Fig. 2H−J and Fig. S3D). The average body weight of mice did not change significantly in either group (Fig. S3E). These findings suggest that *SUV39H1* plays a crucial role in promoting ccRCC growth.

Several forms of regulated cell death (RCD), including apoptosis, necroptosis, pyroptosis, ferroptosis and autophagy-dependent cell death, have been well-characterized[29]. We next attempted to determine whether *SUV39H1* depletion inhibits ccRCC tumor growth by inducing any of these forms of RCD. To test this, five different RCD-specific small-molecule compounds were used to inhibit individual cell death pathways. The death of *SUV39H1*-depleted cells was significantly reduced by treatment with ferrostatin-1, an inhibitor of ferroptosis, suggesting that *SUV39H1* knockdown may attenuate cell growth partly by inducing ferroptosis (Fig. 2K−M and Fig. S3F). To confirm this finding, we assessed intracellular iron, lipid ROS levels and the morphological changes in ccRCC cells. As expected, we found that *SUV39H1* knockdown increased intracellular lipid ROS, mitochondrial superoxide levels, intracellular iron and Fe^{2+} levels, and induced ferroptosis associated morphological changes in ccRCC cells (Fig. 2N−S and Fig. S3G−S3K). Together, our

Table 2 Multivariate Cox regression analysis for overall survival and recurrence-free survival in 358 ccRCC patients.

Characteristic	Overall survival			Recurrence-free survival		
	HR	(95% CI)	*P*	HR	(95% CI)	*P*
SUV39H1 in cancer tissues						
Low	1			1		
High	4.678	1.851−11.821	0.001*	2.420	1.183−4.949	0.016*
TNM stage						
I+II	1			1		
III+IV	4.373	2.373−8.058	<0.001*	3.336	1.754−6.346	<0.001*
Fuhrman grade						
I+II	1			1		
III+IV	1.981	1.216−3.225	0.006*	1.924	1.174−3.154	0.009*
Tumor size (cm)						
≤4	1			1		
>4	3.891	2.081−7.274	<0.001*	5.064	2.676−9.582	<0.001*

HR, hazard ratio; 95% CI, 95% confidence interval. *$P < 0.05$ was considered statistically significant.

Table 3 Comparison of the predictive accuracies of prognostic factors.

Model	Overall survival (n = 358)		Recurrence free survival (n = 358)	
	C-index	AIC	C-index	AIC
SUV39H1	0.628	780.1949	0.600	828.7987
TNM stage	0.589	771.5985	0.576	816.8801
TNM stage+SUV39H1	0.688	752.7648	0.652	808.8266
Fuhrman grade	0.614	788.2059	0.609	825.5831
Fuhrman grade+SUV39H1	0.696	767.8118	0.665	817.0112
Tumor size	0.683	766.2329	0.703	793.0312
Tumor size+SUV39H1	0.748	742.5755	0.749	781.6016
Nomogram	0.791	722.4722	0.782	768.5916
SSIGN	0.678	768.2519	0.702	789.5096

AIC, Akaike information criterion; C-index: Harrell's concordance index.

results suggest that *SUV39H1* knockdown attenuates tumor growth partly by inducing ferroptotic cell death in ccRCC.

3.4. *Inhibition of SUV39H1 enzymatic activity induces ferroptosis and suppresses cell proliferation in ccRCC cells*

To determine whether SUV39H1 enzymatic activity participates into ferroptosis, we examined the effect of the SUV39H1 inhibitor chaetocin on ccRCC cell ferroptosis[30]. Western blot analysis was performed to evaluate the effect of chaetocin on H3K9me3 levels in ccRCC cells. As shown in Supporting Information Fig. S4A, chaetocin treatment reduced the level of H3K9me3 in ccRCC cells. Importantly, we found ferrostatin-1 significantly reduced the cell death induced by chaetocin (Fig. 3A and Fig. S4B). Importantly, electron microscopy analysis indicated that chaetocin treatment significantly induces ferroptosis specific changes of mitochondria such as the disappearance of the mitochondrial crest and increased dense of mitochondrial membrane (Fig. 3B). In addition, chaetocin treatment also increased intracellular levels of lipid ROS, mitochondrial superoxide, iron and Fe^{2+} levels, and induced ferroptosis associated morphological changes in ccRCC cells (Fig. 3C−H and Fig. S4C−S4I). Since chaetocin is a non-selective histone lysine methyltransferase inhibitor (targeting for Suv39H1, G9a and DIM5), we next to test whether the inhibition of G9a or DIM5 impacts the occurrence of ferroptosis in ccRCC. We firstly examined the impacts of G9a inhibition on intracellular iron level, lipid ROS level and the morphology of ccRCC cells with a G9a-selective inhibitor (UNC0638), and found that G9a has no significant impact on ferroptosis-specific phenotypes in ccRCC (Supporting Information Fig. S5). Besides, we found *DIM5* gene is not detected in *Homo sapiens*[31]. These results together largely exclude that the impacts of chaetocin was *via* other targets like G9a and DIM5. Together, we reveal that the inhibition of SUV39H1 enzymatic activity could induce ccRCC cell ferroptosis.

To evaluate whether *SUV39H1* could serve as a potential therapeutic target for ccRCC treatment, we examined the effect of chaetocin on ccRCC cell growth. *In vitro* experiments showed that chaetocin inhibited ccRCC cell proliferation and colony formation, and increased cell death in a dose-dependent manner (Fig. 3I and J and Supporting Information Fig. S6A). Consistent with this, chaetocin treatment significantly increased the proportion of ccRCC cells that arrested in the G2/M phase of the cell cycle (Fig. 3K−L, Fig. S6B and S6C). To assess the anti-tumor effects of chaetocin *in vivo*, we treated a patient-derived xenograft (PDX) ccRCC model with chaetocin and found chaetocin treatment resulted in substantially inhibited tumor growth, as indicated by tumor volume, size and weight (Fig. 3M−O). In terms of tolerance and toxicity, no significant weight loss was observed in either group (Fig. S6D). In summary, our results show that inhibiting SUV39H1 enzymatic activity induces ferroptosis and suppresses ccRCC tumor growth, indicating that SUV39H1 may be an effective therapeutic target for treating ccRCC.

Given that *SUV39H1* depletion also induces G2/M cell cycle arrest, we next asked whether cell cycle arrest is mediated by ferroptosis. Result showed that the inhibition of ferroptosis barely impacts the occurrence of G2/M cell cycle arrest, indicating the regulation of cell cycle is independent of ferroptosis in *SUV39H1* suppressed ccRCC cells (Supporting Information Fig. S7). Considering apoptosis is a key pattern of inducing tumor cell death, we further asked whether cell apoptosis is involved in the *SUV39H1*-induced cell death. Our data indicate that knockdown or inhibition of *SUV39H1* has no significant impact on apoptosis phenotype of ccRCC cells (Supporting Information Fig. S8). Besides, we want to know whether *SUV39H1* knockdown or inhibition have cell cytotoxicity in the normal kidney cell line HK-2. Results showed that *SUV39H1* knockdown or inhibition of SUV39H1 enzymatic activity by chaetocin have some extent effect of cell cytotoxicity in HK-2 cells, which is relatively marginal compared with that in ccRCC cells (Supporting Information Fig. S9). Taken together, our data showed that targeting *SUV39H1* has a potential value in treating ccRCC.

3.5. *SUV39H1 inhibition upregulates DPP4 in ccRCC*

To identify the molecular signaling pathway involved *SUV39H1*-mediated regulation of ferroptotic cell death, we performed an RNA-seq analysis of 786-O cells after *SUV39H1* knockdown. Heat-map analysis of differentially expressed genes (DEGs) showed the overall changes (Fig. 4A). Given the functional role of *SUV39H1* in transcriptional repression of target genes, DEGs that were upregulated following *SUV39H1* knockdown were selected for further analysis. GO enrichment and KEGG pathway analyses were performed to evaluate the functional role of *SUV39H1* in ccRCC. The GO analysis results showed that the upregulated DEGs were enriched with proteins involved in the endoplasmic reticulum lumen, and the KEGG analysis indicated that *SUV39H1* may participate in lysosome function and sphingolipid metabolism in ccRCC (Fig. 4B and C), which have been previously reported play a critical role in ferroptosis[19,32,33].

We next sought to identify the potential targeted genes that may contribute to ferroptosis induction in ccRCC. An ever-expanding number of regulators, such as *GPX4*, *FTH1*, *SLC7A11*, *TFRC* and *DPP4*, are consecutively reported to involve in modulating ferroptosis[19,29]. We found two ferroptosis associated genes (*TFRC* and *DPP4*) expression levels were significantly changed among the Top200 upregulated DEGs (ranked by *P*adj) in response to *SUV39H1* knockdown (Supporting Information Table S9). Next, RT-qPCR was performed to verify the expression level of *TFRC* and *DPP4*, as well as *GPX4*, *FTH1* and *SLC7A11*, and we found that *DPP4* was the most significantly upregulated gene after *SUV39H1* knockdown (Fig. 4D). To

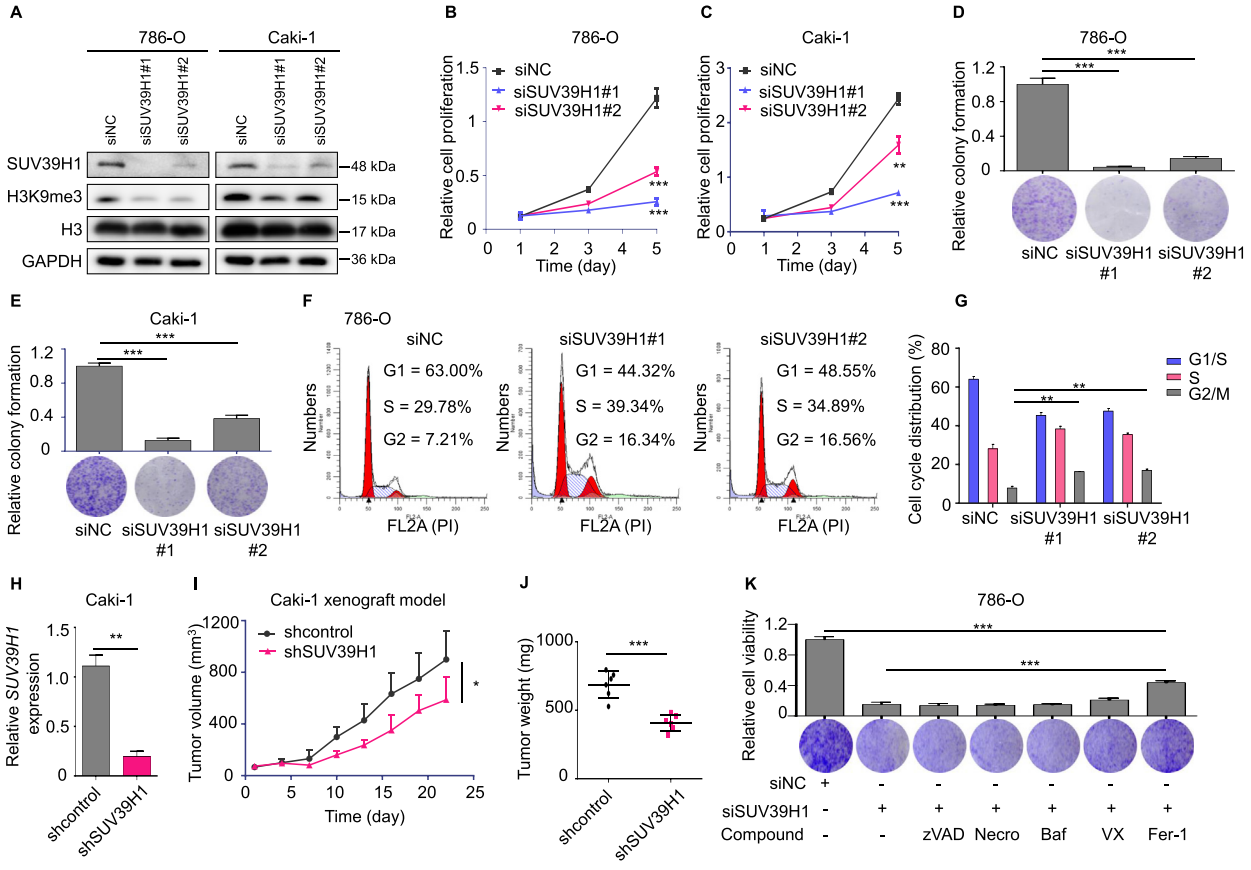

Figure 2 Knockdown of *SUV39H1* attenuates cell growth and induces ferroptotic cell death. (A) Knockdown of *SUV39H1* by specific siRNAs in ccRCC cells, after 48 h, and the expression of SUV39H1, H3K9me3, H3 and GAPDH were detected by Western blot. (B) and (C) Knockdown of *SUV39H1* suppressed cell growth ability in ccRCC cells (786-O and Caki-1). *SUV39H1* was knocked down with *SUV39H1* siRNAs and OD values were used to compare cell growth ability between different groups. Data was presented as mean ± SD, $n = 3$. (D) and (E) Knockdown of *SUV39H1* suppressed 786-O or Caki-1 cell colony formation ability. Three view fields were selected to count the number of cells and data was presented as mean ± SD. (F) and (G) Knockdown of *SUV39H1* significantly induced G2/M cell cycle arrest in 786-O cells. The experiment was repeated three times and data was presented as mean ± SD. (H) RT-qPCR analysis was performed to detect the level of *SUV39H1* mRNA in Caki-1 cells transfected with the *SUV39H1*-specific shRNA and control (shcontrol). Data was presented as mean ± SD, $n = 3$. (I) and (J) Tumor growth curves in *SUV39H1* stable depleted Caki-1 xenograft models, and tumor weights were expressed as mean ± SD, $n = 6$ for each group. (K) Treatment with RCD specific inhibitors, including z-VAD-FMK (an apoptosis inhibitor, 10 μmol/L), necrostatin 1 (a necroptosis inhibitor, 20 μmol/L), bafilomycin A1 (an autophagy inhibitor, 100 nmol/L), VX-765 (a pyroptosis inhibitor, 5 μmol/L), and ferrostatin-1 (a ferroptosis inhibitor, 5 μmol/L), in *SUV39H1* specific siSUV39H1#1 transfected 786-O cells, and cell proliferation was evaluated after 3 days. Three view fields were selected to count the number of cells and data was presented as mean ± SD. (L) and (M) 786-O and Caki-1 cells were transfected with *SUV39H1* specific siRNA (siSUV39H1#1) or negative siRNA (siNC) in the presence and absence of 5 μmol/L Fer-1 (ferrostatin-1), and cell proliferation was evaluated after 3 days. Three view fields were selected to count the number of cells and data was presented as mean ± SD. (N) and (O) Levels of lipid ROS were analyzed in *SUV39H1*-depleted Caki-1 cells. Data was presented as mean ± SD, $n = 3$. (P) and (Q) Levels of mitochondrial superoxide were analyzed in *SUV39H1*-depleted Caki-1 cells. Data was presented as mean ± SD, $n = 3$. (R) and (S) Levels of Fe^{2+} and total iron were analyzed in Caki-1 cells transfected with the *SUV39H1*-specific shRNA and control (shcontrol). Data was presented as mean ± SD, $n = 3$. $^*P < 0.05$, $^{**}P < 0.01$, and $^{***}P < 0.001$.

confirm this finding, we performed Western blot analyses to detect DPP4 protein expression levels in *SUV39H1* deficiency cells. Consistently, DPP4 was significantly upregulated in *SUV39H1*-depleted or inhibition cells compared with the negative control cells (Fig. 4E and F). These data indicate that *DPP4* was transcriptionally upregulated when *SUV39H1* expression was suppressed.

As SUV39H1 primarily catalyzes H3K9me3 status, we next asked whether SUV39H1 modulates the H3K9me3 status of the *DPP4* promoter to regulate its expression. To test this, we performed ChIP-qPCR analysis in ccRCC cells upon *SUV39H1* depletion or inhibition. The results show that H3K9me3 modification in the *DPP4* promoter region was noticeably decreased following *SUV39H1* knockdown or inhibition (Fig. 4G and H). Taken together, these data suggest that *SUV39H1* suppression decreased H3K9me3 localization to the *DPP4* promoter region, which in turn led to the transcriptional upregulation of DPP4 in ccRCC cells.

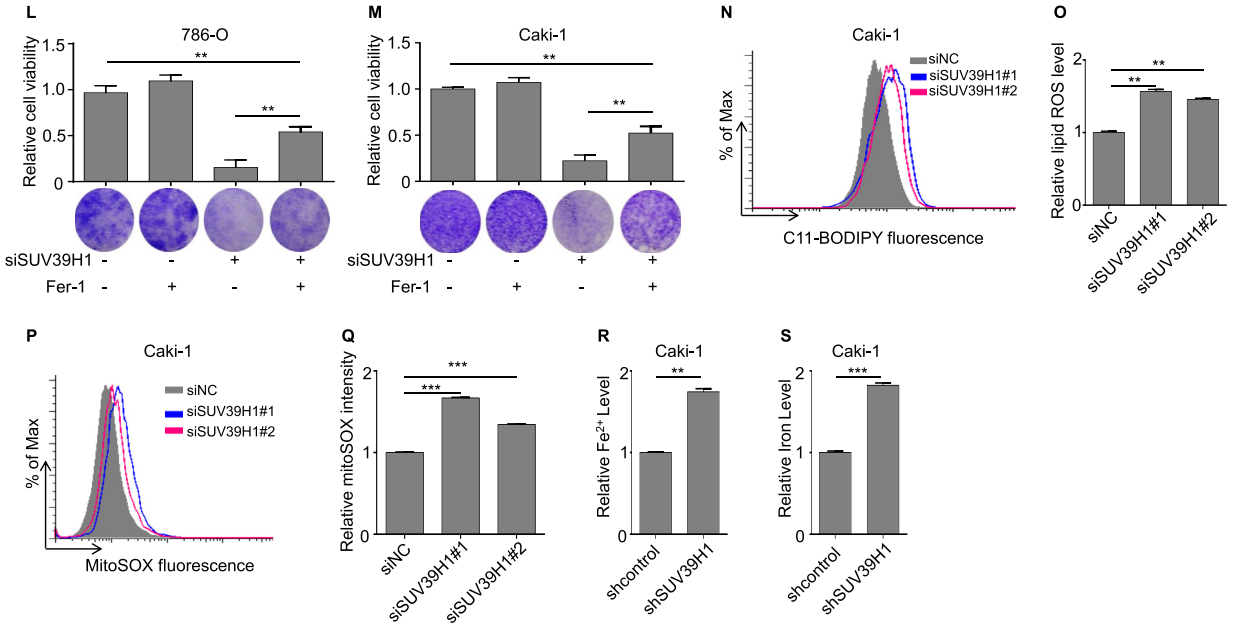

Figure 2 *(continued).*

3.6. SUV39H1 deficiency induces ferroptosis and inhibits cell proliferation by targeting DPP4

Previously report showed that DPP4 plays differential regulation roles of ferroptosis dependent on its subcellular localization in cells and *P53* status[20]. We first detected the subcellular localization of the upregulated DPP4 protein in ccRCC cells, and result showed that *SUV39H1* deficiency increased the expression of DPP4 in both membrane and nuclear of ccRCC cells (Supporting Information Fig. S10A). We next want to figure out whether the *P53* status impacts the DPP4-induced ferroptosis in ccRCC cells. Two ccRCC cell lines 786-O (mutant P53) and Caki-1 (wild-type P53) were used in our study and both cell lines showed ferroptosis after *SUV39H1* depleted, which indicated that the regulation role of DPP4 is independent of *P53* status in ccRCC cells[34]. Together, our data indicate that *SUV39H1* deficiency upregulate the expression of membrane and nucleus DPP4, which is *P53*-independent in ccRCC.

Given that membrane DPP4 contributes the occurrence of ferroptosis *via* cooperating with NOX1, we next to investigate the association between upregulated DPP4 and NOX1 activity in *SUV39H1* deficient ccRCC cells. We observed that NOX activity was remarkably upregulated in 786-O cells following *SUV39H1* depleted (Supporting Information Fig. S10B and S10C), indicating DPP4 may interact with NOX1 to induce ferroptosis in *SUV39H1* deficient ccRCC cells. To determine whether inhibiting DPP4 expression or activity could reverse *SUV39H1*-mediated ferroptosis and its associated phenotypes, we performed DPP4 knockdown or enzyme activity inhibition experiments in *SUV39H1*-deficient ccRCC cells. Vildagliptin was used to specifically inhibit DPP4 enzyme activity. Knockdown of DPP4 expression restored the intracellular lipid ROS, mitochondrial superoxide, iron and Fe^{2+} levels in ccRCC cells (Fig. 5A−F). Furthermore, DPP4 knockdown or enzyme inhibition partially restored cell growth in *SUV39H1*-deficient ccRCC cells (Fig. 5G−I and Supporting Information Fig. S11A−S11E). These findings suggest that *DPP4* is the functional target gene in *SUV39H1*-mediated ferroptosis and its associated phenotypes in ccRCC.

Based on the above findings, we next asked whether DPP4 expression is associated with ccRCC prognosis. The role of DPP4 in ccRCC is poorly understood. We found that ccRCC patients in the TCGA dataset with low *DPP4* transcript levels had a poor prognosis, with a median OS of 38.5 months compared with 42.3 months in the high *DPP4* expression group (Fig. 5J). Finally, patients with a high level of *SUV39H1* expression and a low level of *DPP4* expression had an even worse prognosis (Fig. 5K and Fig. S11F). Additionally, we also evaluated H3K9me3 and DPP4 expression level in the chaetocin-treated group and control group tumor tissues by IHC and verified that chaetocin treatment was associated with obviously increased DPP4 expression (Fig. 5L). Taken together, our findings outline a functional role for the *SUV39H1*−*DPP4* axis in ccRCC progression (Fig. 5M). Loss of *SUV39H1* function in ccRCC tumors leads to hypomethylation of the *DPP4* promoter, upregulating DPP4 expression, which then induces ferroptosis and suppresses cell proliferation. Our data indicate that *SUV39H1* may serve as a therapeutic target for ccRCC treatment.

4. Discussion

Aberrant histone modification is one of the most common events observed in carcinogenesis[35,36]. As a H3K9 methyltransferase, *SUV39H1* has been reported to function as an oncogene in many tumors. However, the exact role of *SUV39H1* in ccRCC progression remains poorly understood. In the present study, we show that *SUV39H1* plays a critical role in ccRCC progression and prognosis, and impacts tumor growth by regulating ferroptotic cell death. By analyzing data from the public TCGA database and our own ccRCC cohorts, we found that *SUV39H1* is overexpressed in ccRCC tumors, and that *SUV39H1* expression levels are significantly correlated with shortened OS and RFS in ccRCC patients.

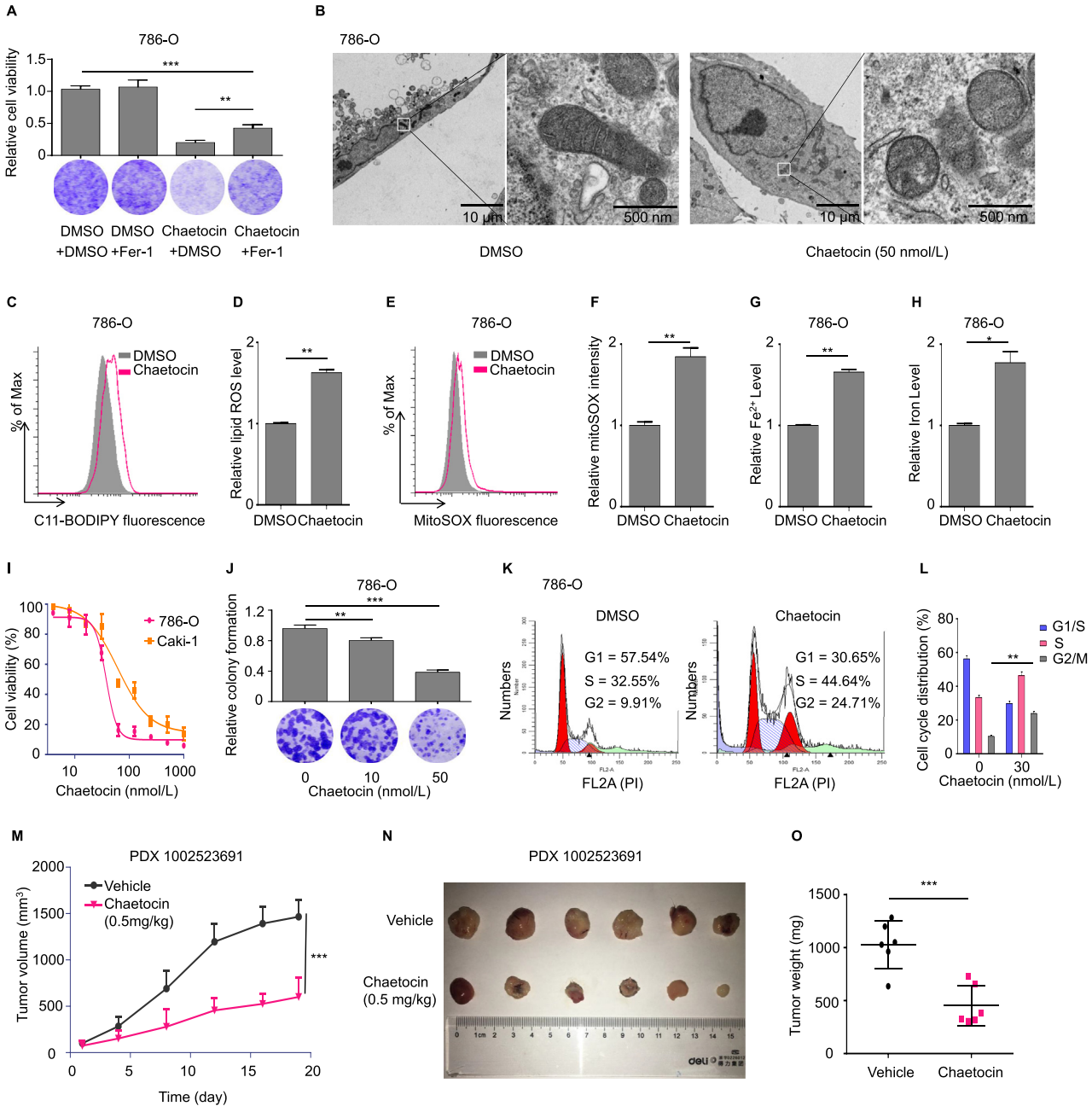

Figure 3 Inhibition of SUV39H1 enzymatic activity induces ferroptosis and suppresses cell proliferation. (A) 786-O cells were treated with chaetocin (80 nmol/L) or DMSO in the presence and absence of 5 μmol/L Fer-1 (ferrostatin-1), and cell proliferation was evaluated after 3 days. Three view fields were selected to count the number of cells and data was presented as mean ± SD. (B) Transmission electron microscopy analysis of 786-O cells treated with DMSO (24 h) and chaetocin (50 nmol/L, 24 h). (C) and (D) Levels of lipid ROS were analyzed in chaetocin (100 nmol/L) treated 786-O cells. Data was presented as mean ± SD, $n = 3$. (E) and (F) Levels of mitochondrial superoxide were analyzed in chaetocin (100 nmol/L) treated 786-O cells. Data was presented as mean ± SD, $n = 3$. (G) and (H) Levels of Fe^{2+} and total iron were analyzed in chaetocin (100 nmol/L) treated 786-O cells. Data was presented as mean ± SD, $n = 3$. (I) Cell proliferation assay was performed to determine the proliferation ability of ccRCC cells (786-O and Caki-1) treated with chaetocin for 5 days in a dose-dependent manner. The experiment was repeated three times and data was presented as mean ± SD. (J) Treatment with chaetocin suppressed 786-O cell colony formation ability. Three view fields were selected to count the number of cells and data was presented as mean ± SD. (K) and (L) Treatment with chaetocin (30 nmol/L) significantly induced G2/M cell cycle arrest in 786-O cells. Data was presented as mean ± SD, $n = 3$. (M) Tumor growth curves in chaetocin (0.5 mg/kg/day) treated ccRCC PDX animal model (PDX 1002523691). $n = 6$ for each group. (N) and (O) Representative photographs of ccRCC PDX animal model tumor tissues treated with chaetocin, and tumor weights were expressed as mean ± SD, $n = 6$ for each group. $^{*}P < 0.05$, $^{**}P < 0.01$, and $^{***}P < 0.001$.

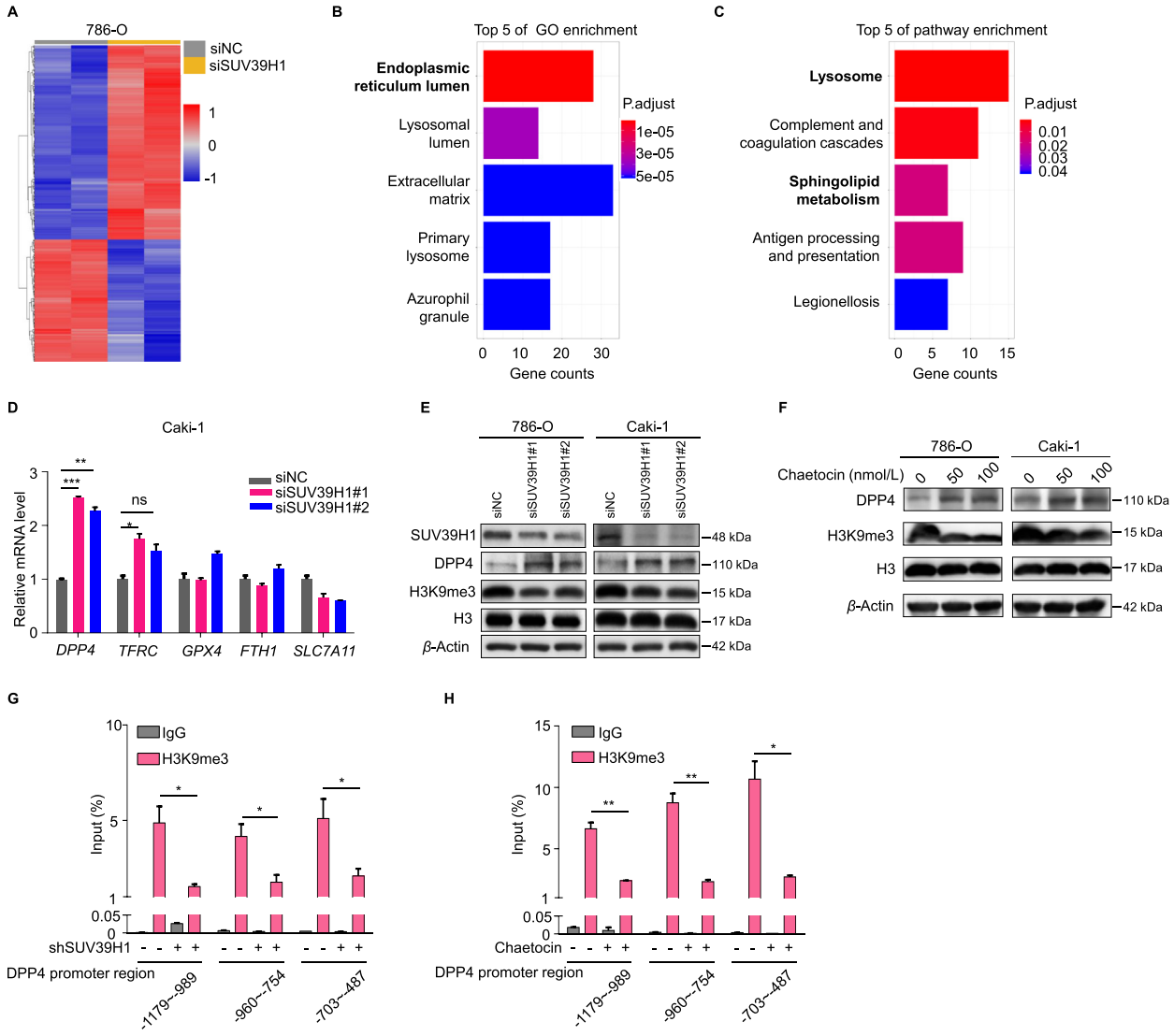

Figure 4 *SUV39H1* deficiency upregulates DPP4 expression in ccRCC. (A) RNA-seq analysis was performed to analyze gene expression changes in 786-O cells transfected with the *SUV39H1* specific siSUV39H1#1 or negative siRNA (siNC), and upregulated genes presented in red while downregulated genes in blue. $n = 2$ for each group. (B) GO functional annotation for upregulated genes in DEGs following *SUV39H1* knockdown. Top 5 of GO enrichments were showed. (C) KEGG functional annotation for upregulated genes in DEGs following *SUV39H1* knockdown. Top 5 of KEGG enrichments were showed. (D) Ferroptosis associated key regulators, including *TFRC*, *DPP4*, *GPX4*, *FTH1* and *SLC7A11*, were verified by RT-qPCR experiment in *SUV39H1* deleted Caki-1 cells. Data was presented as mean ± SD, $n = 3$. (E) DPP4 expression levels were detected by Western blot in *SUV39H1* knockdown ccRCC cells. (F) DPP4 expression levels were detected by Western blot in ccRCC cells treated with different concentrations of chaetocin. (G) H3K9me3 binding at the three sections of *DPP4* promoter in SUV39H1 knockdown 786-O cells. Data was presented as mean ± SD. (H) H3K9me3 binding at the three sections of *DPP4* promoter in chaetocin (100 nmol/L) treated 786-O cells after 3 days. Data was presented as mean ± SD, $n = 3$. *$P < 0.05$, **$P < 0.01$, and ***$P < 0.001$.

We further showed that integrating assessment of *SUV39H1* expression level with several prognostic factors could predict clinical outcomes in ccRCC patients with greater accuracy than the conventional SSIGN prognostic model. In addition, we demonstrated that knocking down *SUV39H1* expression or pharmacologically inhibiting SUV39H1 activity suppresses ccRCC cell growth *in vitro* and *in vivo*. Furthermore, *DPP4*, a well-known ferroptosis regulator, was identified as the direct functional target of *SUV39H1* in mediating ccRCC cell proliferation. Thus, our findings provide an insight into the functional role of *SUV39H1* in ccRCC progression and prognosis, and suggest that *SUV39H1* could be used as a prognostic marker for ccRCC progression and a therapeutic target for ccRCC treatment.

Our data show that *SUV39H1* is mostly overexpressed in ccRCC tissues while a small number of patients may have low expression of *SUV39H1*. Typically, the reason for this phenomenon may due to the heterogeneity of ccRCC. As is a highly heterogeneous and complex disease, ccRCC patients are always facing limited effective treatment options. Therefore, there is an urgent need for improved outcome prediction models to guild clinical decisions following surgery. To this end, numerous nomogram models have been proposed to predict ccRCC clinical

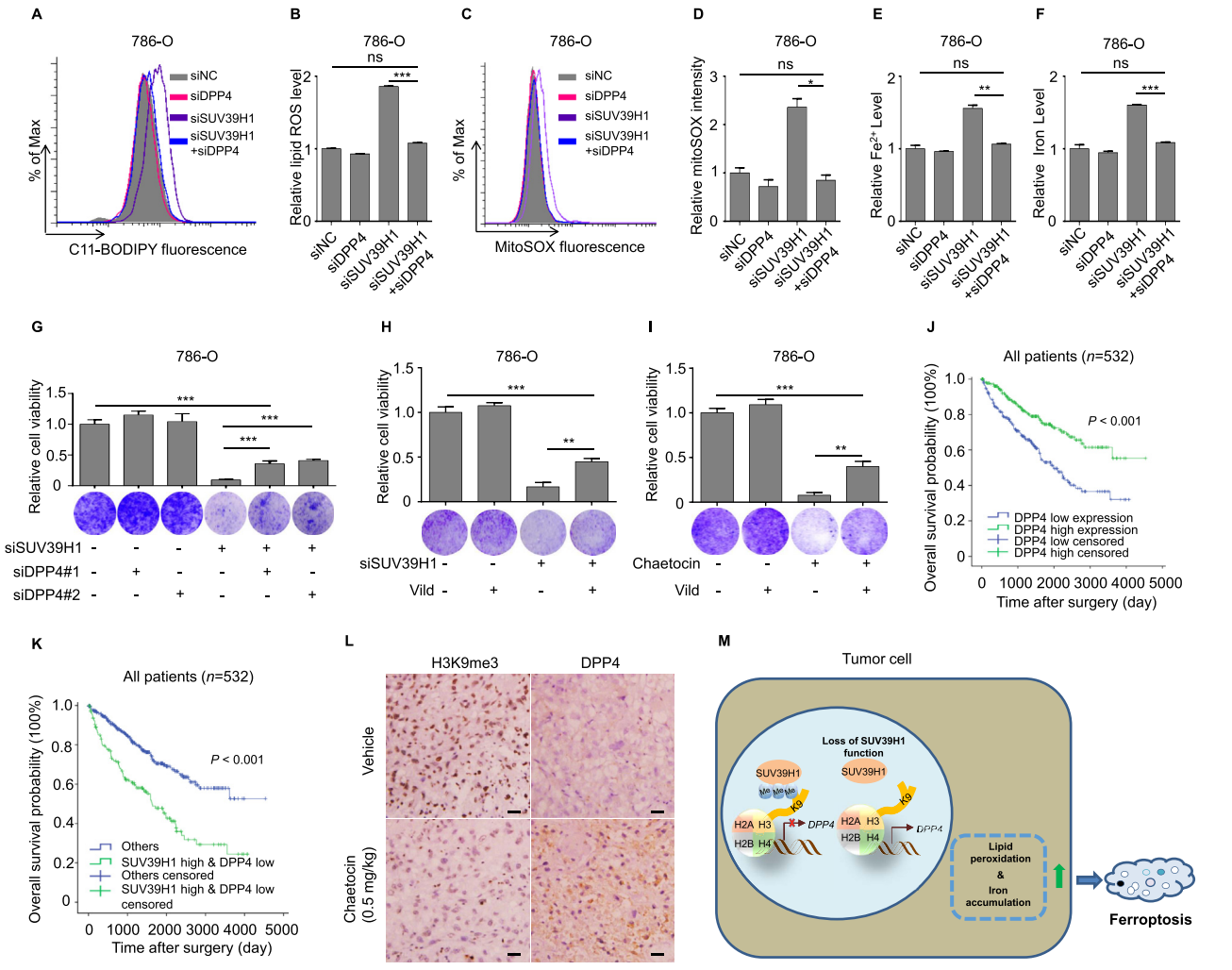

Figure 5 SUV39H1 deficiency induces ferroptosis and inhibits cell proliferation by targeting *DPP4*. (A) and (B) Levels of lipid ROS were analyzed in 786-O cells transfected with the *SUV39H1*-specific siSUV39H1#1 and/or *DPP4*-specific siDPP4#1. Data was presented as mean ± SD, $n = 3$. (C) and (D) Levels of mitochondrial superoxide were analyzed in 786-O cells transfected with the *SUV39H1*-specific siSUV39H1#1 and/or *DPP4*-specific siDPP4#1. Data was presented as mean ± SD, $n = 3$. (E) and (F) Levels of Fe^{2+} and total iron were analyzed in 786-O cells transfected with the *SUV39H1*-specific siSUV39H1#1 and/or *DPP4*-specific siDPP4#1. Data was presented as mean ± SD, $n = 3$. (G) Cell proliferation was evaluated in 786-O cells transfected with *SUV39H1* specific siSUV39H1#1 and/or *DPP4*-specific siRNAs after 3 days. Three view fields were selected to count the number of cells and data was presented as mean ± SD. (H) 786-O cells were transfected with *SUV39H1* specific siSUV39H1#1 or negative siRNA (siNC) in the presence and absence of 10 μmol/L Vild (vildagliptin), and cell proliferation was evaluated after 3 days. Three view fields were selected to count the number of cells and data was presented as mean ± SD. (I) 786-O cells treated with chaetocin (80 nmol/L) or DMSO in the presence and absence of 10 μmol/L Vild (vildagliptin), and cell proliferation was evaluated after 3 days. Three view fields were selected to count the number of cells and data was presented as mean ± SD. (J) Kaplan−Meier analysis of OS for all ccRCC patients with low or high *DPP4* expression level in TCGA dataset. $n = 532$. (K) *SUV39H1* and *DPP4* prognostic interactions. Kaplan−Meier analysis was performed to show the association between OS and *SUV39H1* high & *DPP4* low expression levels in ccRCC patients in TCGA. $n = 532$. (L) IHC analysis of tissues harvested from the mouse tumor model stained for H3K9me3 and DPP4 (scale bar: 10 μm). (M) Schematic diagram depicting the regulation of *DPP4* in ccRCC cells. *SUV39H1* is an epigenetic repressor to suppress DPP4 expression. Loss function of *SUV39H1* in ccRCC tumors contributes the hypomethylation of the *DPP4* promoter to upregulate DPP4 expression and induces *DPP4*-mediated ferroptosis to suppress cell proliferation. Each experiment was performed three times, and data was presented as mean ± SD. $^*P < 0.05$, $^{**}P < 0.01$, and $^{***}P < 0.001$.

outcomes[37−39]. Unfortunately, many of these models have innate limitations, such as insufficient validation and poor accuracy[40]. Here, we found that SUV39H1 expression level is an independent prognostic factor for ccRCC patient outcome. SUV39H1 expression levels were especially accurate in predicting outcomes in ccRCC patients with a high histological grade, intermediate and advanced tumor stages, large tumors, deep invasion, and no lymph node metastasis, suggesting that analysis of SUV39H1 expression may be most appropriate for predicting prognosis in this subset of ccRCC patients. Importantly, when combined with several clinical features, analyzing SUV39H1 expression levels could predict ccRCC patient outcomes with greater accuracy than the

conventional SSIGN prognostic model, which is a powerful predictor of prognosis in ccRCC patients who have undergone radical nephrectomy[37]. Ideally, with more and more external validations of our findings, we believe that SUV39H1 could be considered as a powerful predictor of prognosis in ccRCC patients.

Recently, ferroptosis has been identified as a nonapoptotic form of cell death that is involved in the progression of many diseases, especially cancer[18,41]. Inducing ferroptosis using small molecules is a focus of intense investigation in the cancer therapy field[42]. Although many molecular factors are involved in ferroptosis, several key regulators, such as RAS and TP53, play critical roles in tumor development[19]. However, the correlation between epigenetic alterations and ferroptosis remains poorly understood. Here we show that *SUV39H1* deficiency increases intracellular lipid ROS, mitochondrial superoxide and iron levels, indicating that the HMTase SUV39H1 may regulate ferroptosis in ccRCC cells. More importantly, sorafenib, a first-line clinical drug for advanced ccRCC treatment, is also a ferroptosis inducer, which suggests that the SUV39H1 inhibitor chaetocin could be effective in treating sorafenib-resistant ccRCC patients. Our findings provide the insight into the role of epigenetic alteration in regulating ferroptosis, as well as the biological processes underlying ccRCC progression.

Loss function of *GPX4* is a canonical way to induce ferroptosis. GPX4 is a member of the GSH peroxidases that protects biomembranes against peroxidation damage through repressing phospholipid hydroperoxide[43]. However, our RNA-seq data show that there is no significant expression change for *GPX4* after *SUV39H1* knockdown. Additionally, DPP4, an important ferroptosis-associated regulator that binds to NOX1 to form the DPP4−NOX1 complex, which facilitates lipid peroxidation in ferroptosis, plays a key role in the clinical progression of ccRCC[20]. DPP4 is primarily located at the plasma membrane, where it functions as a serine exopeptidase that cleaves X-proline dipeptides from the N-terminus of polypeptides[44]. In addition to its role in diabetes[45], the biological role of DPP4 in various types of cancers, including ccRCC, has also been investigated. DPP4 activity is negatively correlated with tumor grade and positively correlated with survival in ccRCC patients[46,47]. In our study, we demonstrated that *SUV39H1* deficiency upregulated DPP4 expression. Knocking down DPP4 expression or inhibiting DPP4 enzyme activity restored intracellular lipid ROS and iron levels, and partially restored cell growth in *SUV39H1*-deficient ccRCC cells, suggesting that *DPP4* is a functional target of *SUV39H1* in mediating ccRCC ferroptosis and cell proliferation. Furthermore, we found that *SUV39H1* deficiency upregulates DPP4 expression by decreasing H3K9me3 levels at the *DPP4* promoter. Taken together, these results demonstrate that *SUV39H1* negatively regulates DPP4 expression by modulating H3K9me3 levels at the *DPP4* promoter during ccRCC cell growth. Thus, our study provides a mechanistic insight into the impact of *SUV39H1* on ccRCC tumor growth, which may provide a strategy for ccRCC treatment.

Although our study presents meaningful findings regarding the role of *SUV39H1* in ccRCC progression, it does have several limitations. Specifically, the role of *SUV39H1* expression level in the clinical behavior of ccRCC was investigated by retrospectively analyzing data from TCGA and our own ccRCC cohort. However, the clinical features of our cohort were somewhat different from those of the patients in the TCGA database, so we were unable to analyze enough patients with advanced disease to confirm the role of *SUV39H1* expression levels in advanced ccRCC. Thus, data from multicentric cohorts with comprehensive clinical information are needed to confirm our findings. Besides, we used chaetocin as the inhibitor to inhibit SUV39H1 enzymatic activity. However, chaetocin is a non-selective histone lysine methyltransferase inhibitor which targeted SUV39H1, G9a and DIM5 at the same time. Although we excluded the potential interferences in our study, a SUV39H1-specific inhibitor is still needed to confirm our finding. Additionally, our data show that suppressing ferroptosis only partially restored cell growth in *SUV39H1*-deficient ccRCC cells, suggesting the *SUV39H1* may also regulate ccRCC cell proliferation through other ferroptosis-independent mechanisms. As shown in our data, *SUV39H* deficiency could also induce G2/M cell cycle arrest, which is independent of ferroptosis. Thus, the potential involvement of other molecular mechanisms involved in *SUV39H1* function in ccRCC needs to be explored further.

In conclusion, our study provides the mechanistic insight into *SUV39H1*-dependent epigenetic regulation of ccRCC tumor growth, indicating that *SUV39H1* may serve as a prognostic biomarker for ccRCC progression and a therapeutic target for ccRCC treatment.

Acknowledgments

This study was supported by the advanced technology promotion project of Shanghai Municipal Commission of Health and Family Planning (No. 27 HYR 2013, China) and Doctoral Innovation Fund Projects from Shanghai Jiao Tong University School of Medicine (BXJ201919, China).

Author contributions

Yiran Huang, Jin Zhang and Wei Xue conceived and designed the experiments; Jianfeng Wang, Xiaomao Yin and Wei He performed the experiments, analyzed the data, wrote and validated the paper. All authors read and approved the final manuscript.

Conflicts of interest

The authors declare no conflicts of interest.

Appendix A. Supporting information

Supporting data to this article can be found online at https://doi.org/10.1016/j.apsb.2020.09.015.

References

1. Hsieh JJ, Purdue MP, Signoretti S, Swanton C, Albiges L, Schmidinger M, et al. Renal cell carcinoma. *Nat Rev Dis Primers* 2017;**3**:17009.
2. Rini BI, Campbell SC, Escudier B. Renal cell carcinoma. *Lancet* 2009;**373**:1119−32.
3. Capitanio U, Montorsi F. Renal cancer. *Lancet* 2016;**387**:894−906.
4. Kotecha RR, Motzer RJ. Towards individualized therapy for metastatic renal cell carcinoma. *Nat Rev Clin Oncol* 2019;**16**:621−33.
5. Posadas EM, Limvorasak S, Figlin RA. Targeted therapies for renal cell carcinoma. *Nat Rev Nephrol* 2017;**13**:496−511.
6. Joosten SC, Smits KM, Aarts MJ, Melotte V, Koch A. Epigenetics in renal cell cancer: mechanisms and clinical applications. *Nat Rev Urol* 2018;**15**:430−51.

7. Chen L, Chen L, Qin Z, Lei J, Ye S, Zeng K, et al. Upregulation of miR-489-3p and miR-630 inhibits oxaliplatin uptake in renal cell carcinoma by targeting OCT2. *Acta Pharm Sin B* 2019;**9**:1008−20.
8. Liu B, Wang Z, Zhang L, Ghosh S, Zheng H, Zhou Z. Depleting the methyltransferase Suv39h1 improves DNA repair and extends lifespan in a progeria mouse model. *Nat Commun* 2013;**4**:1868.
9. O'Carroll D, Scherthan H, Peters AH, Opravil S, Haynes AR, Laible G, et al. Isolation and characterization of Suv39h2, a second histone H3 methyltransferase gene that displays testis-specific expression. *Mol Cell Biol* 2000;**20**:9423−33.
10. Vandel L, Nicolas E, Vaute O, Ferreira R, Ait-Si-Ali S, Trouche D. Transcriptional repression by the retinoblastoma protein through the recruitment of a histone methyltransferase. *Mol Cell Biol* 2001;**21**: 6484−94.
11. Rao VK, Pal A, Taneja R. A drive in SUVs: from development to disease. *Epigenetics* 2017;**12**:177−86.
12. Chiba T, Saito T, Yuki K, Zen Y, Koide S, Kanogawa N, et al. Histone lysine methyltransferase SUV39H1 is a potent target for epigenetic therapy of hepatocellular carcinoma. *Int J Canc* 2015;**136**:289−98.
13. Lu C, Yang D, Klement JD, Oh IK, Savage NM, Waller JL. SUV39H1 represses the expression of cytotoxic T-lymphocyte effector genes to promote colon tumor immune evasion. *Canc Immunol Res* 2019;**7**: 414−27.
14. Yang Z, He L, Lin K, Zhang Y, Deng A, Liang Y, et al. The KMT1A-GATA3-STAT3 circuit is a novel self-renewal signaling of human bladder cancer stem cells. *Clin Canc Res* 2017;**23**:6673−85.
15. Kim G, Kim JY, Lim SC, Lee KY, Kim O, Choi HS. SUV39H1/DNMT3A-dependent methylation of the RB1 promoter stimulates PIN1 expression and melanoma development. *FASEB J* 2018;**32**:5647−60.
16. Dixon SJ, Lemberg KM, Lamprecht MR, Skouta R, Zaitsev EM, Gleason CE, et al. Ferroptosis: an iron-dependent form of non-apoptotic cell death. *Cell* 2012;**149**:1060−72.
17. Hirschhorn T, Stockwell BR. The development of the concept of ferroptosis. *Free Radic Biol Med* 2019;**133**:130−43.
18. Stockwell BR, Friedmann Angeli JP, Bayir H, Bush AI, Conrad M, Dixon SJ, et al. Ferroptosis: a regulated cell death nexus linking metabolism, redox biology, and disease. *Cell* 2017;**171**:273−85.
19. Zhou B, Liu J, Kang R, Klionsky DJ, Kroemer G, Tang D. Ferroptosis is a type of autophagy-dependent cell death. *Semin Canc Biol* 2019; **S1044−579X**:30006−9.
20. Xie Y, Zhu S, Song X, Sun X, Fan Y, Liu J, et al. The tumor suppressor p53 limits ferroptosis by blocking DPP4 activity. *Cell Rep* 2017;**20**: 1692−704.
21. Zhang S, Chang W, Wu H, Wang YH, Gong YW, Zhao YL, et al. Pan-cancer analysis of iron metabolic landscape across the Cancer Genome Atlas. *J Cell Physiol* 2020;**235**:1013−24.
22. Wang J, Xu Y, Zhu L, Zou Y, Kong W, Dong B, et al. Cannabinoid receptor 2 as a novel target for promotion of renal cell carcinoma prognosis and progression. *J Canc Res Clin Oncol* 2018;**144**:39−52.
23. Wang J, Xu Y, Zhu L, Zou Y, Kong W, Dong B, et al. High expression of stearoyl-CoA desaturase 1 predicts poor prognosis in patients with clear-cell renal cell carcinoma. *PLoS One* 2016;**11**:e0166231.
24. Hang J, Hu H, Huang J, Han T, Zhuo M, Zhou Y, et al. Sp1 and COX2 expression is positively correlated with a poor prognosis in pancreatic ductal adenocarcinoma. *Oncotarget* 2016;**7**:28207−17.
25. Wang C, Jiang H, Jin J, Xie Y, Chen Z, Zhang H, et al. Development of potent type i protein arginine methyltransferase (PRMT) inhibitors of leukemia cell proliferation. *J Med Chem* 2017;**60**:8888−905.
26. Zhu L, Wang J, Kong W, Huang J, Dong B, Huang Y, et al. LSD1 inhibition suppresses the growth of clear cell renal cell carcinoma *via* upregulating P21 signaling. *Acta Pharm Sin B* 2019;**9**:324−34.
27. Weiss A, Chavez-MacGregor M, Lichtensztajn DY, Yi M, Tadros A, Hortobagyi GN, et al. Validation study of the American Joint Committee on Cancer eighth edition prognostic stage compared with the anatomic stage in breast cancer. *JAMA Oncol* 2018;**4**:203−9.
28. Xiong Y, Liu L, Xia Y, Wang J, Xi W, Bai Q, et al. Low CCL17 expression associates with unfavorable postoperative prognosis of patients with clear cell renal cell carcinoma. *BMC Canc* 2017;**17**:117.
29. Tang D, Kang R, Berghe TV, Vandenabeele P. The molecular machinery of regulated cell death. *Cell Res* 2019;**29**:347−64.
30. Lai YS, Chen JY, Tsai HJ, Chen TY, Hung WC. The SUV39H1 inhibitor chaetocin induces differentiation and shows synergistic cytotoxicity with other epigenetic drugs in acute myeloid leukemia cells. *Blood Canc J* 2015;**5**:e313.
31. Zhang X, Tamaru H, Khan SI, Horton JR, Keefe LJ, Selker EU, et al. Structure of the neurospora SET domain protein DIM-5, a histone H3 lysine methyltransferase. *Cell* 2002;**111**:117−27.
32. Lee YS, Lee DH, Choudry HA, Bartlett DL, Lee YJ. Ferroptosis-induced endoplasmic reticulum stress: cross-talk between ferroptosis and apoptosis. *Mol Canc Res* 2018;**16**:1073−6.
33. Novgorodov SA, Voltin JR, Gooz MA, Li L, Lemasters JJ, Gudz TI. Acid sphingomyelinase promotes mitochondrial dysfunction due to glutamate-induced regulated necrosis. *J Lipid Res* 2018;**59**:312−29.
34. Berglind H, Pawitan Y, Kato S, Ishioka C, Soussi T. Analysis of p53 mutation status in human cancer cell lines: a paradigm for cell line cross-contamination. *Canc Biol Ther* 2008;**7**:699−708.
35. Dawson MA, Kouzarides T. Cancer epigenetics: from mechanism to therapy. *Cell* 2012;**150**:12−27.
36. Chen X, Pan X, Zhang W, Guo H, Cheng S, He Q, et al. Epigenetic strategies synergize with PD-L1/PD-1 targeted cancer immunotherapies to enhance antitumor responses. *Acta Pharm Sin B* 2020;**10**: 723−33.
37. Frank I, Blute ML, Cheville JC, Lohse CM, Weaver AL, Zincke H. An outcome prediction model for patients with clear cell renal cell carcinoma treated with radical nephrectomy based on tumor stage, size, grade and necrosis: the SSIGN score. *J Urol* 2002;**168**:2395−400.
38. Karakiewicz PI, Briganti A, Chun FK, Trinh QD, Perrotte P, Ficarra V, et al. Multi-institutional validation of a new renal cancer-specific survival nomogram. *J Clin Oncol* 2007;**25**:1316−22.
39. Leibovich BC, Blute ML, Cheville JC, Lohse CM, Frank I, Kwon ED, et al. Prediction of progression after radical nephrectomy for patients with clear cell renal cell carcinoma: a stratification tool for prospective clinical trials. *Cancer* 2003;**97**:1663−71.
40. Leibovich BC, Lohse CM, Cheville JC, Zaid HB, Boorjian SA, Frank I, et al. Predicting oncologic outcomes in renal cell carcinoma after surgery. *Eur Urol* 2018;**73**:772−80.
41. Lu B, Chen XB, Ying MD, He QJ, Cao J, Yang B. The role of ferroptosis in cancer development and treatment response. *Front Pharmacol* 2017;**8**:992.
42. Liang C, Zhang X. Recent progress in ferroptosis inducers for cancer therapy. *Adv Mater* 2019;**31**:e1904197.
43. Seibt TM, Proneth B, Conrad M. Role of GPX4 in ferroptosis and its pharmacological implication. *Free Radic Biol Med* 2019;**133**:144−52.
44. Matteucci E, Giampietro O. Dipeptidyl peptidase-4 (CD26): knowing the function before inhibiting the enzyme. *Curr Med Chem* 2009;**16**: 2943−51.
45. Liu J, Huan Y, Li C, Liu M, Shen Z. Establishment of a selective evaluation method for DPP4 inhibitors based on recombinant human DPP8 and DPP9 proteins. *Acta Pharm Sin B* 2014;**4**:135−40.
46. Larrinaga G, Blanco L, Sanz B, Perez I, Gil J, Unda M, et al. The impact of peptidase activity on clear cell renal cell carcinoma survival. *Am J Physiol Ren Physiol* 2012;**303**:F1584−91.
47. Varona A, Blanco L, Perez I, Gil J, Irazusta J, Lopez JI, et al. Expression and activity profiles of DPP IV/CD26 and NEP/CD10 glycoproteins in the human renal cancer are tumor-type dependent. *BMC Canc* 2010;**10**:193.